RESEARCH ARTICLE

SAMRIDDHI Volume 14, Issue 1, 2022 Print ISSN: 2229-7111 Online ISSN: 2454-5767

Multi-spectral Image Fusion using Wavelet Transform

Mitul M. Patel*, Arvind R. Yadav

E&C Engg. Department, Parul Institute of Engineering & Technology, Parul University, Gujrat, India

Abstract

The fusion of visible and infrared images of the same scene results in a single fused image that can provide a more detailed interpretation of the situation. With the help of energy compression and multiresolution characteristics of wavelets, which fuse the salient features such as edges and textures from source images without introducing any artifacts for context improvement and situational awareness, image fusion is more effective. This paper combines visible and infrared images (LWIR and NIR) using different wavelet transform methods on night-time imagery up to the 8th level of image decomposition. The performance of various wavelet techniques for multi-spectral image fusion was evaluated based on subjective and objective parameters. Additionally, Petrovic Metric parameters are used to measure the fusion performance.

Keywords: Multi-spectral image fusion, Night time images, Wavelet transform.

SAMRIDDHI : A Journal of Physical Sciences, Engineering and Technology (2022); DOI: 10.18090/samriddhi.v14i01.15

Introduction

Image fusion is often implemented on signal, feature, and decision processing levels. The lowest level of image fusion is signal-level image fusion, also known as pixel-level image fusion. The method of fusing visual information associated with each pixel from several registered images into a single fused image is known as signal-level image fusion. Pixel-level image fusion is a subdomain of multisensory information fusion, a field that has gained much attention in the previous two decades.

Object-level image fusion, also known as salient feature-level image fusion, combines information derived from individual input images such as feature, object names, and property descriptors. Decision or symbol level image fusion is the highest level of fusion, probabilistic decision information derived by local decision-makers based on the outcomes of feature level processing on image data generated by individual sensors. It is extremely difficult to extract all important information from visible images in poor lighting conditions, such as low night-time illumination and dense fog/smoke.

Now a days, the widespread infrared imaging systems provide an effective solution to this task. Infrared cameras are able to acquire the thermal information of a scene. Because of its various spectrums, infrared imaging is usually not preferred by the human visual system, leading to loss of spatial information and unnatural visual quality. By generating a fused image, infrared and visible image fusion tries to take advantage of the necessary qualities of these two imaging techniques, which clearly capture thermal targets and perceptually amusing backgrounds. Multi-spectral image fusion has several benefits to real-world applications, like video surveillance, object identification, and face recognition.[5,8,13] The intensity of infrared and visible images at the same location often change rapidly due to differences in imaging mechanisms. Most of the infrared and visible image fusion algorithms are introduced multi-scale to pursue perceptually good results. To obtain a perceptually good fused image, the majority of infrared and visible image fusion algorithms are introduced in a multi-scale approach. The input images are translated into a transform domain first, and then the decomposed coefficients are combined using some predefine fusion rules. Finally, the fused image is obtained by executing the inverse transform.[1,5,10,12] The major contribution of this research article is mainly divided among methodology of multi-spectral image fusion in the transform domain,Fusion Technique using pixel significance, Experimental results and conclusion.

Corresponding Author: Mitul M. Patel, E&C Engg. Department, Parul Institute of Engineering & Technology, Parul University, Gujrat, India, e-mail: mitul.patel@paruluniversity.ac.in

How to cite this article: Patel, M.M., & Yadav, A.R. (2022). Multi-spectral Image Fusion using Wavelet Transform. *SAMRIDDHI : A Journal of Physical Sciences, Engineering and Technology,* 14(1), 93-102.

Source of support: Nil

Conflict of interest: None

Methodology of Multi-Spectral Image Fusion

The discrete wavelet transform is used in pixel-level image fusion to produce fused images with more information than the input images, making them more suitable for human visual perception, object detection, and target recognition. It is essential for multi-spectral image fusion have to be correctly aligned input images a pixel-by-pixel basis. [1,2,5,14] Here we assume that the input images are perfectly registered. Figure 1 shows general image fusion framework using discrete wavelet transform.

Step 1: To ensure that the corresponding pixels are aligned, the input images to be fused must be registered.

Step 2: Input images are decomposed into wavelet transformed images, separately, based on wavelet transformation. The transformed images with k-level decomposition will include one low-frequency direction (Approximate band) and three high-frequency directions (horizontal, vertical, and diagonal).

Step 3: A specific fusion rule is used to combine the wavelet coefficients of distinct portions or bands.

Step 4: An inverse wavelet transform based on the combined wavelet coefficients from Step 3 is utilized to create the fused image.

Fusion Technique

The Fusion Technique, which determines how to integrate the wavelet coefficients in a suitable way to achieve a high-quality fused image, is the primary step in wavelet-based image fusion, which should be given more attention. Various fusion rules have been proposed, divided into a pixel-based method and a window-based method.[3,10,11] The commonly known pixel-based image fusion rule was used. This approach may select the important features from the input images, but it requires high contrast and is vulnerable to noise and artifacts. As a result, certain noise and artifacts are easily added to the fused image, reducing the quality of the fused image. Another pixel-based method is the averaging fusion rule, which can help to stabilize the image fusion result. This technique introduces the blurring effect and lowers the contrast in the fused image.[10,13]

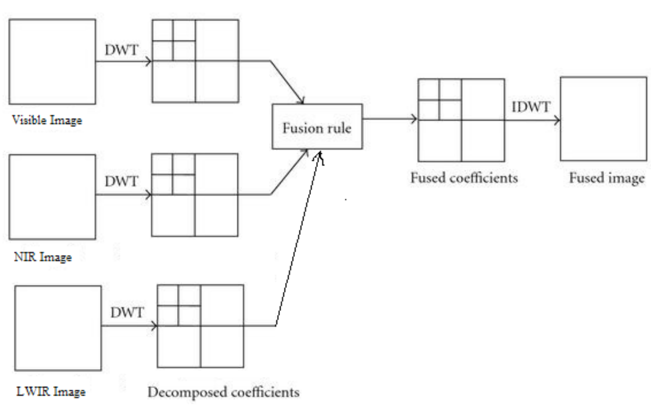

Figure 1: General wavelet-based image fusion scheme [1,2]

More complex fusion rules such as window-based or region-based are also proposed because these types of schemes are more robust than the pixel-based scheme against the image misregistration. Burt presented a weighted average fusion rule based on windows. However, the weights in this approach are based on a user-defined threshold.[4] By examining the maximum absolute variance value of the central coefficients inside a window, Li et al. employed an area-based maximum selection rule to identify which of the input is likely to contain the most useful information. However, this method has been proved better than the pyramid-based method. The demerit of this method is that it considers both low-frequency and high-frequency band wavelet coefficients in the same way.[6] However, in many applications, a human is the ultimate user or interpreter of the fused image. As a result, while fusing images, human perception should be taken into account. Human eyes have distinct sensitivity to wavelet coefficients of a low-resolution and high-resolution band, according to HVS theoretical models.[7,15]

The multi-resolution decomposition generates four bands at each level (A, H, V, and D). H, V, and D represent horizontal, vertical, and diagonal detail information, respectively. A means an approximate and scaled-down version of the input image and is used for further decomposition. Let us sub-bands indicated by B_K. where B can be replaced A, H, V, D. The suffix 'k' indicates how many decomposition stages that specific band can be found in.

In level 3 sub bands, the significance (weight) S of a detail coefficient B_3 takes into account the coefficient as well as all of the children's and grandchildren's coefficients and is calculated as follows [3], [10], [13]:

$$S_{B_3}(i,j) = |B_3(i,j)| + \sum_{m=0}^{1}\sum_{n=0}^{1} |B_2(2i-m, 2j-n)| + \sum_{r=0}^{3}\sum_{s=0}^{3} |B_2(4i-r, 4j-s)| \tag{1}$$

Because the coefficients in level 2 sub-band B_2 do not have grandchildren, the significance S is calculated as follows:

$$S_{B_3}(i,j) = |B_3(i,j)| + \sum_{m=0}^{1}\sum_{n=0}^{1} |B_2(2i-m, 2j-n)| + \sum_{r=0}^{3}\sum_{s=0}^{3} |B_2(4i-r, 4j-s)| \tag{2}$$

The average energy over a brief area of window size w x w around that location is utilized to compute the significance S because the coefficient in level 1 sub-bands B_1 does not have both children and grandchildren.

$$S_{B_1}(i,j) = \frac{\sum_{m=-(w-1)/2}^{(w-1)/2} \sum_{n=-(w-1)/2}^{(w-1)/2} B_1{}_{(i-m,j-n))^2}}{w^2} \tag{3}$$

Because the coefficients in approximate band A_3 do not have both children and grandchildren, the significance S of a coefficient in an approximate band is calculated using the significance S of the relevant coefficients in detail sub bands H_3, V_3, and D_3.

$$S_{A_3}(i,j) = S_{H_3}(i,j) + S_{V_3}(i,j) + S_{D_3}(i,j) \tag{4}$$

These significances are determined for all input images A, B, and C (visible, NIR and LWIR) (visible, NIR and LWIR). The weighted average of three input images is determined as the fused coefficient f(i,j), where Sa, Sb, and Sc are the significance of the coefficients a(i,j), b(i,j), and c(i,j) pertaining to respective input images A,B, and C:

$$f(i,j) = \frac{a(i,j)S_a + b(i,j) + c(i,j)S_c}{S_a + S_b + S_c} \tag{5}$$

Experimental Results

The ground truth is unknown in most applications, making evaluating fusion performance problematic. Researchers have designed and used a number of metrics to assess fusion performance. Several traditional quality and quantity parameters that have been previously stated in the literature are evaluated for a full research. Conventional performance measures average pixel intensity (API), standard deviation (SD), average gradient (AG), entropy (H), mutual information (MI), fusion symmetry (FS), correlation coefficient (CC), spatial frequency (SF) and Petrovic metric parameter $Q^{\frac{ABC}{F}}$ (total information transferred from source images to the fused image), $L^{\frac{ABC}{F}}$ (total loss of information) and $N^{\frac{ABC}{F}}$ (noise or artifacts added in a fused image due to fusion process)and a sum of all three should result in unity.[3,10,11,16]

The TRICLOBS (TRI-band color low-light obServation) dataset was used for short-range surveillance applications. TRICLOBS (TRI-band color low-light Observation) is a dynamic multi-band image data set of sixteen motion sequences in the visible (0.4–0.7m), near-infrared (NIR, 0.7–1.0m), and long-wave infrared (LWIR, 8–14m) bands. The database contains three different situations that reflect various military and civilian surveillance scenarios. People (military and civilian) who are motionless, walking or jogging, or carrying various objects are shown in the scenes. The scenes also include vehicles, greenery, buildings, or other man-made things. TRICLOBS Data set is available from the Fig share Repository: (http://dx.doi.org/10.6084/m9.figshare.3206887).[15]

Tables 1, 2, and 3 of various multi-spectral images list traditional performance measurements such as API, SD, AG, H, MI, FS, CC, SF, and objective performance measures. The quality of the fused image should theoretically improve as the value of these parameters increases $Q^{\frac{ABC}{F}}$, $L^{\frac{ABC}{F}}$ and $N^{\frac{ABC}{F}}$, where it should be low. The higher the value of a traditional performance metric and lower the value of an objective performance measure are bolded in all Tables. For performance comparison of Multispectral

Table 1: Performance comparison of Kaptein_1123 images

Wavelet	*L*	*API*	*SD*	*AG*	*H*	*MIF*	*FS1*	*FS2*	*CC*	*SF*	*Q*	*L*	*N*
db8	1	**90.43**	34.72	8.03	**6.85**	2.83	1.79	1.91	0.69	11.62	0.61	0.35	0.27
	2	83.29	32.77	6.42	6.70	3.33	1.83	1.76	**0.71**	8.88	0.59	0.40	0.10
	3	81.73	32.02	6.28	6.66	3.32	1.83	1.76	0.70	8.77	0.60	0.40	0.07
	4	81.20	32.53	6.28	6.72	3.37	1.83	1.74	**0.71**	8.78	0.60	0.40	0.07
	5	80.87	32.43	6.27	6.66	3.41	**1.86**	1.73	0.69	8.78	0.61	0.39	0.06
	6	81.91	32.43	6.27	6.70	3.45	1.84	1.74	**0.71**	8.78	0.61	0.39	0.06
	7	81.22	32.36	6.28	6.70	3.48	1.85	1.73	0.70	8.79	0.61	0.39	0.07
	8	81.67	32.34	6.28	6.69	3.47	1.85	1.74	0.70	8.79	0.61	0.39	0.06
db16	1	89.77	33.45	7.85	6.81	2.71	1.78	1.90	0.69	10.84	**0.56**	0.40	0.27
	2	82.00	31.97	6.33	6.66	3.26	1.83	1.76	0.70	8.71	0.57	0.43	0.09
	3	81.60	32.37	6.24	6.70	3.34	1.83	1.75	0.70	8.69	0.59	0.41	0.07
	4	80.98	32.34	6.23	6.68	3.50	**1.86**	1.73	0.70	8.71	0.60	0.40	0.07
	5	82.02	32.51	6.23	6.70	3.44	1.83	1.74	0.70	8.72	0.60	0.40	0.07
	6	82.40	32.61	6.22	6.69	3.50	1.85	1.74	0.70	8.71	0.60	0.40	0.07
	7	81.24	32.70	6.23	6.69	3.48	1.85	1.74	0.70	8.71	0.60	0.40	0.07
	8	81.68	32.43	6.22	6.66	3.46	1.84	1.74	0.70	8.71	0.60	0.40	0.07
coif5	1	90.44	**34.82**	8.09	6.83	2.82	1.78	1.91	0.68	11.68	0.61	0.35	0.29
	2	83.30	32.42	6.35	6.69	3.34	1.83	1.76	**0.71**	8.78	0.58	0.41	0.09
	3	82.29	32.34	6.22	6.67	3.37	1.83	1.75	0.70	8.72	0.60	0.40	0.06
	4	80.79	32.44	6.22	6.71	3.42	1.83	1.74	0.70	8.74	0.61	0.39	0.05
	5	82.05	32.75	6.22	6.69	3.44	1.84	1.74	0.69	8.74	0.61	0.39	0.05
	6	82.68	33.07	6.22	6.70	3.47	1.84	1.75	0.70	8.73	0.61	0.39	0.05
	7	81.90	33.22	6.21	6.71	3.45	1.85	1.74	0.70	8.73	0.61	0.39	0.05
	8	81.68	33.06	6.22	6.71	3.43	1.85	1.74	0.70	8.73	0.61	0.39	0.05

Wavelet	*L*	*API*	*SD*	*AG*	*H*	*MIF*	*FS1*	*FS2*	*CC*	*SF*	*Q*	*L*	*N*
sym8	1	89.71	34.45	**8.46**	6.78	2.80	1.79	1.91	0.68	**12.78**	0.70	**0.26**	0.31
	2	84.04	32.56	6.45	6.71	3.39	1.84	1.76	**0.71**	9.07	0.61	0.38	0.09
	3	84.39	33.08	6.33	6.74	3.48	1.85	1.75	**0.71**	8.97	0.62	0.38	0.07
	4	84.65	34.01	6.31	6.78	3.53	1.85	1.75	**0.71**	8.97	0.63	0.37	0.06
	5	84.39	34.97	6.31	6.80	**3.61**	**1.86**	1.74	**0.71**	8.98	0.63	0.37	0.05
	6	83.29	34.91	6.30	6.80	3.57	1.85	1.74	0.70	8.97	0.63	0.37	0.05
	7	81.06	34.12	6.30	6.79	3.54	**1.86**	1.74	0.70	8.97	0.63	0.37	0.05
	8	81.67	34.00	6.30	6.77	3.53	**1.86**	1.74	0.70	8.97	0.63	0.37	0.05
bior6.8	1	89.81	33.99	8.22	6.80	2.87	1.78	**1.92**	0.68	12.32	0.70	0.27	0.28
	2	83.90	32.32	6.37	6.71	3.42	1.83	1.76	**0.71**	8.87	0.60	0.39	0.08
	3	84.17	32.69	6.27	6.73	3.50	1.84	1.76	**0.71**	8.81	0.62	0.38	0.05
	4	84.23	33.34	6.24	6.74	3.54	1.85	1.76	**0.71**	8.79	0.62	0.38	0.05
	5	83.78	33.64	6.24	6.72	3.52	1.84	1.77	**0.71**	8.78	0.62	0.38	0.05
	6	82.42	33.75	6.23	6.72	3.51	1.84	1.75	**0.71**	8.78	0.62	0.38	0.05
	7	82.02	33.96	6.24	6.73	3.47	**1.86**	1.74	0.70	8.78	0.62	0.38	0.05
	8	81.68	33.80	6.24	6.73	3.46	**1.86**	1.74	0.70	8.78	0.62	0.38	0.05
DCHWT	1	89.86	33.21	7.83	6.76	2.84	1.78	**1.92**	0.70	11.79	0.69	0.28	0.27
	2	83.81	32.40	6.06	6.68	3.39	1.84	1.75	0.70	8.62	0.59	0.40	0.07
	3	83.90	32.63	5.93	6.69	3.53	1.85	1.75	**0.71**	8.53	0.60	0.39	**0.04**
	4	83.89	32.93	5.90	6.69	3.58	**1.86**	1.74	**0.71**	8.52	0.61	0.39	**0.04**
	5	83.83	33.40	5.91	6.72	3.60	**1.86**	1.74	0.70	8.53	0.61	0.39	**0.04**
	6	83.32	33.66	5.92	6.72	3.60	**1.86**	1.73	**0.71**	8.53	0.61	0.39	**0.04**
	7	81.89	32.80	5.90	6.68	3.57	**1.86**	1.73	0.70	8.53	0.61	0.39	**0.04**
	8	81.70	32.91	5.90	6.69	3.5	**1.86**	1.73	0.70	8.53	0.61	0.39	**0.04**

Table. 2: Performance comparison of reek.bmp images

Wavelet	*L*	*API*	*SD*	*AG*	*H*	*MIF*	*FS1*	*FS2*	*CC*	*SF*	*Q*	*L*	*N*
db8	1	97.37	55.85	11.41	7.61	3.89	1.77	1.91	0.77	19.85	0.74	0.23	0.28
	2	88.49	44.50	8.34	7.29	4.02	1.82	1.86	0.77	14.79	**0.66**	0.33	0.09
	3	89.86	33.21	7.83	6.76	2.84	1.78	1.92	0.70	11.79	0.69	0.28	0.27
	4	85.88	44.68	7.86	7.28	4.26	1.79	1.86	0.73	14.76	0.69	0.31	0.06
	5	85.37	46.06	7.84	7.26	4.51	1.80	1.87	0.74	14.78	0.70	0.30	0.06
	6	84.85	45.65	7.83	7.26	4.65	1.79	1.86	0.74	14.78	0.69	0.30	0.06
	7	85.38	46.50	7.83	7.27	**4.71**	1.79	1.86	0.74	14.78	0.70	0.30	0.06
	8	85.89	46.53	7.83	7.26	4.69	1.79	1.87	0.74	14.78	0.70	0.30	0.06
db16	1	98.29	**59.06**	11.32	**7.68**	3.84	1.76	1.94	0.76	18.82	0.72	0.25	0.27
	2	86.75	44.32	8.17	7.30	4.01	1.79	1.88	0.75	14.59	**0.66**	0.34	0.08
	3	86.09	45.41	7.89	7.29	4.25	1.78	1.86	0.73	14.56	0.68	0.32	0.07
	4	85.48	46.16	7.80	7.27	4.56	1.79	1.87	0.74	14.60	0.69	0.31	0.06
	5	86.84	47.01	7.79	7.22	4.67	1.79	1.87	0.74	14.60	0.69	0.31	0.06
	6	86.84	47.01	7.79	7.22	4.67	1.79	1.87	0.74	14.60	0.69	0.31	0.06
	7	85.66	46.70	7.79	7.26	4.68	1.78	1.87	0.74	14.59	0.69	0.31	0.06
	8	85.92	46.71	7.79	7.26	4.67	1.78	1.87	0.74	14.60	0.69	0.31	0.06

Wavelet	*L*	*API*	*SD*	*AG*	*H*	*MIF*	*FS1*	*FS2*	*CC*	*SF*	*Q*	*L*	*N*
coif5	1	97.05	55.05	10.95	7.60	3.86	1.78	1.91	0.77	19.20	0.72	0.25	0.26
	2	88.54	43.95	8.19	7.27	4.02	1.82	1.85	0.77	14.59	**0.66**	0.33	0.09
	3	87.56	44.56	7.85	7.31	4.13	1.80	1.87	0.76	14.60	0.68	0.32	0.06
	4	85.63	44.35	7.74	7.28	4.24	1.80	1.86	0.74	14.59	0.69	0.31	0.06
	5	84.31	45.47	7.71	7.23	4.44	1.80	1.88	0.74	14.65	0.69	0.31	0.06
	6	86.57	46.38	7.71	7.24	4.59	1.79	1.87	0.74	14.65	0.69	0.30	0.06
	7	85.97	46.84	7.71	7.27	4.62	1.79	1.87	0.74	14.65	0.69	0.30	0.06
	8	85.88	46.85	7.71	7.27	4.61	1.79	1.87	0.74	14.65	0.69	0.30	0.06
sym8	1	**98.11**	53.01	**11.52**	7.54	3.96	1.79	1.90	0.77	21.06	0.79	**0.19**	0.25
	2	88.34	43.25	8.43	7.26	3.89	1.84	1.84	**0.78**	15.11	0.69	0.31	0.09
	3	89.48	44.35	8.04	7.29	4.00	1.82	1.86	0.77	14.94	0.69	0.30	0.06
	4	89.98	45.68	7.93	7.30	4.21	1.82	1.87	0.75	14.96	0.70	0.30	0.06
	5	89.25	46.42	7.88	7.26	4.52	1.82	1.87	0.75	14.95	0.70	0.29	0.06
	6	88.21	47.97	7.87	7.22	4.58	1.80	1.88	0.74	14.95	0.70	0.29	0.06
	7	85.82	47.44	7.87	7.27	4.64	1.80	1.87	0.74	14.95	0.70	0.29	0.06
	8	85.87	47.30	7.87	7.26	4.62	1.80	1.88	0.74	14.95	0.70	0.29	0.06
bior6.8	1	97.70	51.67	11.50	7.51	3.96	1.79	1.89	0.77	**21.11**	0.79	**0.19**	0.23
	2	88.12	42.84	8.37	7.24	3.93	**1.85**	1.83	**0.78**	14.97	0.69	0.31	0.08
	3	89.41	43.85	7.97	7.28	4.02	1.83	1.85	0.77	14.77	0.70	0.30	0.06
	4	89.92	44.95	7.78	7.30	4.20	1.82	1.87	0.77	14.73	0.70	0.30	0.05
	5	88.66	46.04	7.74	7.28	4.41	1.80	1.88	0.75	14.74	0.70	0.30	0.05
	6	86.38	46.21	7.72	7.27	4.60	1.80	1.87	0.73	14.73	0.70	0.30	0.05
	7	85.72	46.79	7.72	7.28	4.63	1.79	1.87	0.74	14.73	0.70	0.30	0.05
	8	85.86	46.83	7.72	7.28	4.64	1.79	1.87	0.74	14.73	0.70	0.30	0.05
DCHWT	1	97.40	56.86	10.92	7.62	3.79	1.76	**1.97**	0.75	19.74	0.79	**0.19**	0.21
	2	87.89	45.07	7.79	7.26	4.31	1.80	1.87	0.74	14.37	0.68	0.31	0.05
	3	88.22	45.88	7.55	7.25	4.49	1.80	1.87	0.74	14.33	0.69	0.31	**0.04**
	4	88.22	46.43	7.51	7.24	4.58	1.80	1.87	0.74	14.33	0.69	0.31	**0.04**
	5	88.00	46.76	7.51	7.25	**4.71**	1.80	1.86	0.74	14.34	0.69	0.30	**0.04**
	6	87.81	46.95	7.52	7.26	4.68	1.79	1.85	0.73	14.34	0.69	0.30	**0.04**
	7	87.11	48.05	7.53	7.27	4.69	1.79	1.87	0.74	14.35	0.69	0.30	**0.04**
	8	85.92	47.90	7.53	7.31	4.76	1.80	1.86	0.74	14.35	0.69	0.30	**0.04**

Table. 3: Performance comparison of sand path images

Wavelet	*L*	*API*	*SD*	*AG*	*H*	*MIF*	*FS1*	*FS2*	*CC*	*SF*	*Q*	*L*	*N*
db8	1	90.77	24.95	9.69	6.47	2.62	**1.61**	1.81	0.69	11.45	0.72	0.26	0.15
	2	88.90	17.81	9.10	6.14	2.15	1.59	1.90	0.72	10.64	0.67	0.33	0.10
	3	89.08	17.77	9.02	6.14	2.24	1.59	1.91	**0.73**	10.58	0.69	0.31	0.06
	4	89.03	17.73	9.02	6.14	2.27	1.59	**1.92**	**0.73**	10.58	0.69	0.31	0.06
	5	89.55	17.93	9.02	6.15	2.35	1.59	1.91	0.72	10.58	0.69	0.31	0.06
	6	89.16	17.96	9.02	6.16	2.35	1.59	**1.92**	**0.73**	10.58	0.69	0.31	0.06
	7	89.48	18.06	9.02	6.16	2.35	1.59	1.91	**0.73**	10.58	0.69	0.31	0.06
	8	89.30	18.08	9.02	6.16	2.35	1.59	1.91	**0.73**	10.58	0.69	0.31	0.06

db16	1	89.90	23.63	9.55	6.46	2.57	**1.61**	1.81	0.69	11.24	0.71	0.28	0.14
	2	88.96	17.46	9.01	6.12	2.14	1.59	1.91	0.73	10.52	0.66	0.33	0.10
	3	89.17	17.60	8.95	6.12	2.25	1.59	1.91	**0.73**	10.46	0.68	0.32	0.07
	4	89.53	18.02	8.96	6.15	2.34	1.59	1.91	0.72	10.47	0.68	0.32	0.06
	5	89.27	17.66	8.96	6.13	2.31	1.58	**1.92**	**0.73**	10.47	0.68	0.32	0.06
	6	89.17	17.80	8.96	6.14	2.27	1.59	1.91	**0.73**	10.47	0.68	0.32	0.06
	7	89.44	17.88	8.96	6.15	2.29	1.59	1.90	**0.73**	10.47	0.68	0.32	0.06
	8	89.29	17.91	8.97	6.15	2.30	1.59	1.90	**0.73**	10.48	0.68	0.32	0.06
coif5	1	90.81	24.67	9.68	6.46	2.62	**1.61**	1.81	0.69	11.44	0.72	0.27	0.15
	2	88.86	17.69	9.04	6.14	2.16	1.59	1.90	0.72	10.61	**0.66**	0.33	0.09
	3	89.00	17.67	8.98	6.14	2.23	1.59	1.91	**0.73**	10.58	0.68	0.32	0.06
	4	89.15	17.66	8.98	6.14	2.23	1.59	1.91	**0.73**	10.57	0.69	0.31	0.05
	5	89.27	17.81	8.98	6.14	2.33	1.59	**1.92**	**0.73**	10.57	0.69	0.31	0.05
	6	89.02	17.98	8.98	6.16	2.30	1.59	1.91	0.72	10.57	0.69	0.31	0.05
	7	89.12	18.00	8.99	6.16	2.31	1.59	1.91	0.72	10.57	0.69	0.31	0.06
	8	89.30	17.98	8.98	6.16	2.30	1.59	1.91	**0.73**	10.57	0.69	0.31	0.05
sym8	1	**91.68**	**25.83**	**9.90**	**6.48**	**2.66**	**1.61**	1.82	0.68	**11.85**	0.74	0.25	0.14
	2	88.97	17.91	9.11	6.14	2.16	1.60	1.90	0.72	10.73	0.67	0.32	0.09
	3	89.08	18.10	9.07	6.17	2.26	1.59	1.90	0.72	10.70	0.69	0.31	0.06
	4	89.16	18.03	9.07	6.16	2.28	1.59	1.91	**0.73**	10.69	0.69	0.31	0.06
	5	89.25	17.94	9.07	6.16	2.28	1.59	1.91	**0.73**	10.69	0.69	0.31	0.06
	6	89.39	18.05	9.07	6.16	2.28	1.59	1.91	**0.73**	10.69	0.69	0.31	0.06
	7	89.53	18.11	9.07	6.17	2.32	1.59	1.90	0.72	10.69	0.69	0.31	0.06
	8	89.30	18.14	9.07	6.17	2.32	1.59	1.90	**0.73**	10.69	0.69	0.31	0.06
bior6.8	1	91.51	25.10	9.77	6.46	2.65	**1.61**	1.82	0.68	11.68	0.74	**0.25**	0.13
	2	88.87	17.83	9.04	6.14	2.18	1.60	1.90	0.72	10.66	0.67	0.32	0.08
	3	88.95	18.04	9.00	6.16	2.26	1.59	1.90	0.72	10.64	0.69	0.31	0.05
	4	89.03	17.99	9.00	6.16	2.28	1.59	1.90	**0.73**	10.63	0.69	0.31	0.05
	5	89.04	17.88	9.00	6.15	2.28	1.59	1.91	**0.73**	10.63	0.69	0.31	0.05
	6	88.99	17.96	9.00	6.16	2.29	1.59	1.91	**0.73**	10.63	0.69	0.31	0.05
	7	89.06	17.98	9.00	6.16	2.29	1.59	1.91	**0.73**	10.63	0.69	0.31	0.05
	8	89.30	17.96	9.00	6.16	2.29	1.59	1.91	**0.73**	10.63	0.69	0.31	0.05
DCHWT	1	91.54	24.95	9.63	6.45	2.64	**1.61**	1.82	0.68	11.53	0.73	0.26	0.12
	2	88.94	17.79	8.84	6.14	2.17	1.59	1.90	0.72	10.39	0.67	0.33	0.07
	3	88.96	18.02	8.80	6.16	2.28	1.59	1.90	0.72	10.35	0.68	0.32	**0.04**
	4	89.05	18.04	8.80	6.16	2.32	1.59	1.90	0.72	10.35	0.69	0.31	**0.04**
	5	88.96	17.85	8.80	6.15	2.35	1.59	1.91	0.72	10.35	0.69	0.31	**0.04**
	6	88.88	17.94	8.80	6.16	2.35	1.59	1.91	0.72	10.35	0.69	0.31	**0.04**
	7	89.01	17.95	8.80	6.16	2.30	1.59	1.91	**0.73**	10.35	0.69	0.31	**0.04**
	8	89.31	17.98	8.79	6.16	2.29	1.59	1.91	**0.73**	10.35	0.69	0.31	**0.04**

images, 'Kaptein_1123', 'reek', and 'sand path' are used. In 'Kaptein_1123' consist of visible, near-infrared, and long-wave infrared images. The grass, tree, road, door lighting, and object around the door are visible in Kaptein_1123 visible image. Kaptein_1123 near-infrared image contains one person and a light lamp at the top of the door. The smoke is coming outside from the chamber and walking direction of person visibly in Kaptein_1123 long-wave infrared image. In reek, the visible image chair, grass, and curtain of windows are clearly visible. The water cane and wire fencing are clearly visible in the reek near-infrared image. The reek long-wave infrared image contains a solar plate on the roof and pole. The sand path and fencing of wire are available in visible and near-infrared images of the sand path, respectively. Longwave infrared sand path image detect hidden person under forest.[15]

In Figures 2 to 4, despite the fact that all fused images include the majority of the information from the three input

Figure 2: Input Images (a, b, c) and fused images of different wavelets from Level-1 to Level-8

Figure 3: Input Images (a, b, c) and fused images of different wavelets from Level-1 to Level-8

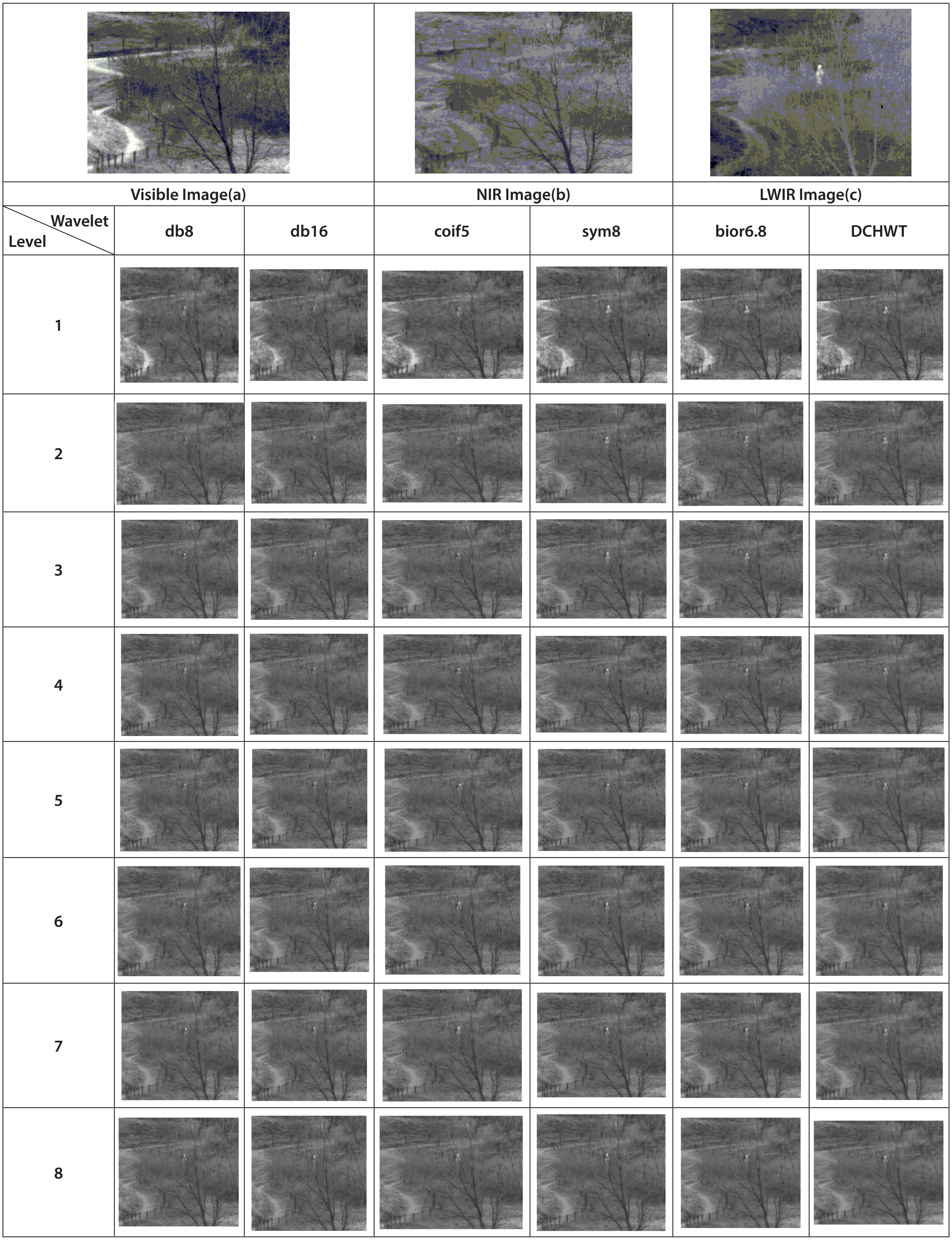

Figure 4: Input Images (a, b, c) and fused images of different wavelets from Level-1 to Level-8

images, some blocking artifacts and haziness can be visible in fused images, as well as some haziness and boundary effects below the 4^{th} level of wavelets. The visual quality of fused images could not improve significantly beyond the $4^{th}/5^{th}$ level of image decomposition; rather same or the lower levels of image decomposition have been stated as shown in Figures 2 to 4. This happens because the sub-images produced by the image decomposition level beyond the $4^{th}/5^{th}$ do not encompass visible qualitative information. Furthermore, adding more levels of picture decomposition increases computing cost (in terms of addition and multiplications) without improving the fused images significantly. Therefore, in this work, the authors have considered up to 8 levels of image decomposition.

Conclusion

In this paper, various wavelets transform (db8, db16, coif5, sym8, bior6.8, and DCHWT) has been used up to 8 levels of image decomposition for fusing multi-spectral nighttime images. Experiments were conducted on TRICLOBS (TRI-band Color Low-light ObServation) dataset for short-range surveillance applications. Fusion performance evaluated using conventional parameters, gradient information based Petrovic Metrics, and visual analysis. The trade-off between fused image quality and computational complexity is stable at the 4^{th} level of image decomposition.

Reference

[1] Toet, A., Van Ruyven, L. J., & Valeton, J. M. (1989). Merging thermal and visual images by a contrast pyramid. Optical engineering, 28(7), 789-792.

[2] Burt, P. J. (1992). A gradient pyramid basis for pattern-selective image fusion. Proc. SID 1992, 467-470.

[3] Li, H., Manjunath, B. S., & Mitra, S. K. (1995). Multisensor image fusion using the wavelet transform. *Graphical models and image processing*, *57*(3), 235-245.

[4] Piella, G. (2003). A general framework for multiresolution image fusion: from pixels to regions. *Information fusion*, *4*(4), 259-280.

[5] Gülzow, T., Ludwig, T., & Heute, U. (2003). Spectral-subtraction speech enhancement in multirate systems with and without non-uniform and adaptive bandwidths. *Signal Processing*, *83*(8), 1613-1631.

[6] Vesteinsson, A., Sveinsson, J. R., Benediktsson, J. A., & Aanaes, H. (2005, July). Spectral consistent satellite image fusion: Using a high resolution panchromatic and low resolution multi-spectral images. In *Proceedings. 2005 IEEE International Geoscience and Remote Sensing Symposium, 2005. IGARSS'05.* (Vol. 4, pp. 2834-2837). IEEE.

[7] Petrovic, V., & Xydeas, C. (2005, October). Objective image fusion performance characterisation. In *Tenth IEEE International Conference on Computer Vision (ICCV'05) Volume 1* (Vol. 2, pp. 1866-1871). IEEE.

[8] Shreyamsha Kumar, B. K., Prabhakar, B., Suryanarayana, K., Thilagavathi, V., & Rajagopal, R. (2006). Target identification using harmonic wavelet based ISAR imaging. *EURASIP Journal on Advances in Signal Processing*, *2006*, 1-13.

[9] Toet, A., & Hogervorst, M. A. (2009, April). TRICLOBS portable triband color lowlight observation system. In *Multisensor, Multisource Information Fusion: Architectures, Algorithms, and Applications 2009* (Vol. 7345, pp. 20-30). SPIE.

[10] Shah, P., Merchant, S. N., & Desai, U. B. (2010). Fusion of surveillance images in infrared and visible band using curvelet, wavelet and wavelet packet transform. International Journal of Wavelets, Multiresolution and Information Processing, 8(02), 271-292.

[11] Shah, P., Srikanth, T. V., Merchant, S. N., & Desai, U. B. (2011, June). A novel multifocus image fusion scheme based on pixel significance using wavelet transform. In *2011 IEEE 10th IVMSP Workshop: Perception and Visual Signal Analysis* (pp. 54-59). IEEE.

[12] Toet, A., & Hogervorst, M. A. (2012). Progress in color night vision. Optical Engineering, 51(1), 010901.

[13] Shah, P., Merchant, S. N., & Desai, U. B. (2013). Multifocus and multispectral image fusion based on pixel significance using multiresolution decomposition. *Signal, Image and Video Processing*, *7*(1), 95-109.

[14] Shreyamsha Kumar, B. K. (2013). Multifocus and multispectral image fusion based on pixel significance using discrete cosine harmonic wavelet transform. *Signal, Image and Video Processing*, *7*(6), 1125-1143.

[15] Toet, A., de Jong, M. J., Hogervorst, M. A., & Hooge, I. T. (2014, February). Perceptual evaluation of colorized nighttime imagery. In *Human Vision and Electronic Imaging XIX* (Vol. 9014, p. 901412). International Society for Optics and Photonics.

[16] Du, J., Li, W., Lu, K., & Xiao, B. (2016). An overview of multi-modal medical image fusion. *Neurocomputing*, *215*, 3-20.

[17] Toet, A., Hogervorst, M. A., & Pinkus, A. R. (2016). The TRICLOBS dynamic multi-band image data set for the development and evaluation of image fusion methods. *PloS one*, *11*(12), e0165016.